


Limit of the two-dimensional linear potential theories on the propulsion of a flapping airfoil in forward flight in terms of the Reynolds and Strouhal number

J. Alaminos-Quesada ^{*}*Fluid Mechanics Group, Universidad de Málaga, Dr Ortiz Ramos s/n, 29071 Málaga, Spain*

(Received 24 May 2021; accepted 1 November 2021; published 9 December 2021)

A sixth-order compact finite differences scheme of the two-dimensional transport-Poisson equations in terms of vorticity-stream function is formulated to solve the motion of a flapping airfoil in a noninertial reference frame, fitting a NACA-0012 profile with the Kármán-Trefftz transformation. These numerical simulations have been used to estimate the validity range of the linear potential theories of Fernandez-Feria and the classical Garrick model on the propulsion of a pitching airfoil pivoting to a quarter chord length of the leading edge and a heaving airfoil in forward flight, in terms of the Reynolds, Re , and Strouhal number, St , compared with available numerical and experimental data. The Fernandez-Feria's propulsion theory shows better agreement with the numerical and experimental results than the Garrick model for the time-averaged thrust coefficient where it is found that the Fernandez-Feria's theory is limited to $Re \gtrsim 4000$ and $St \lesssim 0.25$ for pure pitching motions and $Re \gtrsim 1000$ and $St \lesssim 0.2$ for pure heaving motions.

DOI: [10.1103/PhysRevFluids.6.123101](https://doi.org/10.1103/PhysRevFluids.6.123101)

I. INTRODUCTION

The recent interest in the development of small unmanned aerial and aquatic vehicles bioinspired by small flying animals [1,2] has caused that the unsteady aerodynamics of flapping foils to be a subject of active research. In spite of the great advances in computational fluid dynamics, the linear unsteady potential theory is still a great tool to estimate the aerodynamics forces and moment of flapping airfoils for high Reynolds number and small oscillating amplitudes. The theoretical models has been used widely to compare with numerical and experimental results [1,3–6] in order to validate their results for cases where it is well known that the linear potential theory works well.

The linear potential theory for a heaving and pitching motion of a rigid foil was originally studied in Ref. [7] for lift and moment and in Ref. [8] for thrust and propulsion efficiency. Recently, the linear potential flow theory has been extended for a flapping airfoil in different cases [9–12] with an almost flat wake vortex sheet, using the vortical impulse theory [13,14] in the correct way to obtain the thrust and propulsive efficiency and with the main assumptions of considering high Reynolds. number and small oscillating amplitudes. The classical linear potential theory from Ref. [8] computes the thrust force of a plunging and pitching airfoil in forward flight considering only two effects: the leading-edge suction and the projection in the flight direction of the pressure force on the airfoil. However, the new approach of the linearized propulsion theory [9] takes into account the complete vorticity distribution on the airfoil and the wake, correcting the propulsion force predicted in Ref. [8]. A quite similar vortex theory formulation has been developed in Ref. [15] but considering the trailing wake as a succession of point vortices instead of the continuous

*jalaminos@uma.es

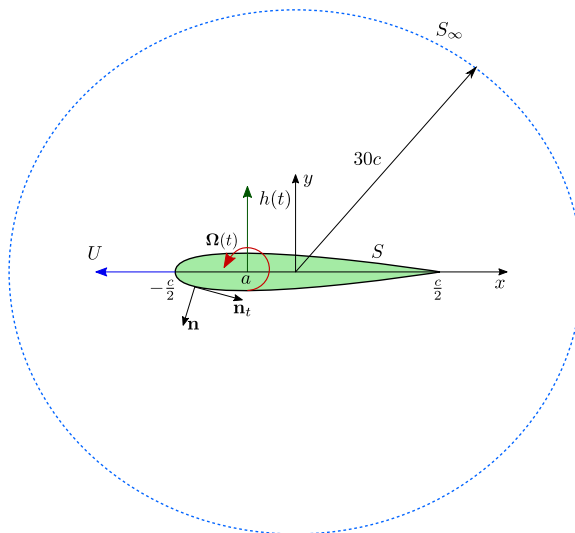


FIG. 1. Schematic of the heaving and pitching airfoil bounded by S and the integration domain delimited by the surfaces S_∞ .

distribution in Ref. [13] to obtain the lift force and moment of an unsteady thin airfoil. In Ref. [16], several semiempirical models and the linear potential theories have been compared for the thrust force and propulsion efficiency of pitching foils. Also, numerical simulations have been done to see the effect of the pivot axis location on its propulsive performance for pitching foils [17] comparing with the linear theories. However, these results are for a fixed Reynolds number. On the other hand, the authors of Ref. [18] have analyzed the effect of the Reynolds number for a pitching airfoil pivoting to a quarter chord length of the leading edge but without comparing with the potential theory.

Thus, the present work focuses on finding the range of validity of the linearized potential theory in terms of Reynolds and Strouhal numbers. For that, a numerical simulation of a flapping airfoil has been implemented, estimating the critical Reynolds and Strouhal numbers from which the linear propulsion theories predict better the temporal evolution or the time-averaged thrust coefficient. Pure motions have been considered: a pure pitching motion pivoting to a quarter chord length, $a = -0.25$, with a pitching amplitude of $a_0 = 2^\circ$, as well as the selected case of $St = 0.2$ varying the pivot point location from the leading edge ($a = -0.5$) to the trailing edge ($a = 0.5$) and a pure heaving motion with a plunging amplitude of $h_0 = 0.025$ (both scaled with the foil's chord length c). The Strouhal number has varied from 0.05 to 0.4, and the Reynolds number has taken the values 500, 1000, 2000, 4000, and 8000 for both motions. Additionally, the main equations in terms of vorticity and stream function which have to be solved to do a numerical simulation of a flapping airfoil in a noninertial reference frame have been developed, fitting a NACA-0012 profile with a conformal mapping.

II. FORMULATION OF THE PROBLEM

A two-dimensional (2D) and incompressible flow is considered over a heaving and pitching airfoil of chord length c that moves with constant speed U along the negative x axis (see Fig. 1). In this reference frame, the motion of the airfoil is given by the vertical displacement of its mean-camber line, i.e.,

$$\mathbf{y}_0(\mathbf{x}, t) = h(t)\mathbf{e}_y + [\alpha(t)\mathbf{e}_z] \wedge \mathbf{x}, \quad \text{with} \quad \mathbf{x} = (x - a)\mathbf{e}_x + y\mathbf{e}_y, \quad (1)$$

and

$$h(t) = h_0 \cos(2kt), \quad \alpha(t) = a_0 \cos(2kt + \phi), \quad (2)$$

where $k = \omega c / (2U)$ is the reduced frequency, with nondimensional period $T = \pi / k$, which consists of a heaving displacement $h(t)$ of amplitude h_0 and a pitching rotation $\alpha(t)$ of amplitude a_0 pivoting at $x = a$ with ϕ the phase shift between the heaving and pitching motions of the foil. Note that the nondimensional coordinate \mathbf{x} and the amplitude of heaving motion, h_0 , is scaled with the foil's chord length c and the time t with c/U . Thus, the corresponding nondimensional velocity of the airfoil, scaled with the velocity U , is given by

$$\mathbf{v}_0(\mathbf{x}, t) = -\mathbf{e}_x + \frac{d\mathbf{y}_0}{dt} = -\mathbf{e}_x + \frac{dh}{dt} \mathbf{e}_y + \boldsymbol{\Omega}(t) \wedge \mathbf{x}, \quad (3)$$

where $\boldsymbol{\Omega}(t) = \frac{d\alpha}{dt} \mathbf{e}_z$ is the pitching rotation velocity, whereas in a noninertial frame, the airfoil does not move and the fluid domain is moving with the opposite velocity of the airfoil, i.e.,

$$\mathbf{u}_\infty(\mathbf{x}, t) = -\mathbf{v}_0(\mathbf{x}, t). \quad (4)$$

As a consequence, the fluid field velocity can be decomposed into two terms,

$$\mathbf{u} = \mathbf{u}_\infty + \mathbf{u}', \quad (5)$$

where \mathbf{u}' is the disturbance in the fluid field velocity. To characterize the motion of the airfoil with the kinematics parameters, the Strouhal number has been selected, i.e.,

$$\text{St} = \frac{fA}{U}, \quad (6)$$

where f is the frequency of the motion, A is the peak-to-peak excursion of the airfoil's trailing-edge, and U is the translating speed. For pure heaving and pure pitching motion, the Strouhal number can be written respectively as

$$\text{St}_{\text{heave}} = \frac{2kh_0}{\pi}, \quad \text{St}_{\text{pitch}} = \frac{2k}{\pi} \left(\frac{1}{2} - a \right) \sin(a_0). \quad (7)$$

A. Governing equations

In the noninertial frame, the nondimensional Navier-Stokes equations are written as

$$\frac{\partial \mathbf{u}}{\partial t} = -\frac{1}{2} \nabla p - \mathbf{u} \cdot \nabla \mathbf{u} + \frac{1}{\text{Re}} \nabla^2 \mathbf{u} - \mathbf{a}_z - \mathbf{a}_{\text{Cor}} - \mathbf{a}_{\text{tan}} - \mathbf{a}_{\text{cen}}, \quad (8)$$

where p is the pressure (without the hydrostatic component) scaled with $\rho U^2 / 2$ where ρ is the fluid density, Re the Reynolds number based on the chord length of the airfoil, \mathbf{a}_y the heaving motion acceleration, $\mathbf{a}_{\text{Cor}} = 2\boldsymbol{\Omega} \wedge \mathbf{u}$ the Coriolis acceleration, $\mathbf{a}_{\text{tan}} = \frac{d\boldsymbol{\Omega}}{dt} \wedge \mathbf{x}$ the tangential acceleration, and $\mathbf{a}_{\text{cen}} = \boldsymbol{\Omega} \wedge (\boldsymbol{\Omega} \wedge \mathbf{x})$ is the centrifugal acceleration. Using the expression of the two-dimensional vorticity $\boldsymbol{\omega} = (\nabla \wedge \mathbf{u}) \mathbf{e}_z$ and noting that the curl of the different accelerations are

$$\nabla \wedge (\mathbf{a}_z) = \nabla \wedge (\mathbf{a}_{\text{Cor}}) = \nabla \wedge (\mathbf{a}_{\text{cen}}) = 0, \quad \nabla \wedge (\mathbf{a}_{\text{tan}}) = 2 \frac{d\boldsymbol{\Omega}}{dt}, \quad (9)$$

with the change of variable

$$\boldsymbol{\omega}' = \boldsymbol{\omega} + 2\boldsymbol{\Omega}(t), \quad (10)$$

Eq. (8) reduces to

$$\frac{\partial \boldsymbol{\omega}'}{\partial t} = -(\nabla \wedge \psi) \cdot \nabla \boldsymbol{\omega}' + \frac{1}{\text{Re}} \nabla^2 \boldsymbol{\omega}', \quad (11)$$

where the stream function, ψ , is defined by $\mathbf{u} = \nabla \wedge (\psi \mathbf{e}_z)$. For convenience, the stream function is separated into background, $\boldsymbol{\psi}$, and disturbance, ψ' , terms, i.e.,

$$\psi = \boldsymbol{\psi} + \psi'. \quad (12)$$

The most convenient choice for the background velocity is the free-stream velocity, \mathbf{u}_∞ , and thus

$$\mathbf{u}_\infty = \nabla \wedge \boldsymbol{\psi}, \quad \mathbf{u}' = \nabla \wedge \psi'. \quad (13)$$

The background stream function, $\boldsymbol{\psi}$, can be obtained directly integrating the velocity Eq. (4), i.e.,

$$\boldsymbol{\psi} = y + \dot{h}(t)x + \dot{\alpha}(t) \left[\frac{y^2}{2} + x \left(\frac{x}{2} - a \right) \right]. \quad (14)$$

On the other hand, for incompressible flows and taking into account the change of variable Eq. (10) and the definition Eq. (12), the continuity equation yields

$$\boldsymbol{\omega}' = -\nabla^2 \psi'. \quad (15)$$

Thus, the problem has been reduced to two analytical expressions, Eq. (10) and Eq. (12), with two partial differential equations: the vorticity transport equation Eq. (11) and a Poisson equation Eq. (15) for the stream function ψ' .

B. Boundary conditions

Boundary conditions are required for $\boldsymbol{\omega}'$ and ψ' in the Eq. (11) and Eq. (15) respectively in order to close the problem. The appropriate boundary conditions at infinity are that the velocity equals the free-stream velocity and the fluid is irrotational in the inertial frame. At the inlet, disturbances to the free-stream flow are neglected, so that the boundary condition for the stream function, ψ' , is given by

$$\left. \frac{\partial \psi'}{\partial n} \right|_{\text{inlet}} = 0, \quad (16)$$

where $\partial/\partial n$ refers to the normal derivative. As the wake is highly unsteady, a much more passive boundary condition is necessary for the outlet. In general, the pressure gradient will be small at the output and it could be neglected. So, if the viscosity is neglected too, the boundary condition at the outlet is given by

$$\left. \frac{D}{Dt} \left(\frac{\partial \psi'}{\partial n} \right) \right|_{\text{outlet}} = 0, \quad (17)$$

which has a similar form to boundary condition for vorticity and allows for some simplification of the numerical procedure. This boundary condition has already been tested for a heaving airfoil at low Reynolds numbers from Ref. [19]. In practice, the simulations are terminated before any significant vorticity becomes close to the outlet boundary. The airfoil surface has to be a streamline, $\partial\psi/\partial s = 0$, which for simplicity is selected, $\psi = 0$, so that the boundary condition for ψ' at the airfoil is $\psi' = -\boldsymbol{\psi}$. In addition, the airfoil is a nonslip surface and for that the vorticity at the airfoil, $\boldsymbol{\omega}_a$, can be related to the total stream function by

$$\boldsymbol{\omega}_a = - \left. \frac{\partial^2 \psi}{\partial n^2} \right|_{\text{airfoil}}. \quad (18)$$

C. Forces and pressure distribution on the surface

Once these equations are solved, one is interested in the force (per unit length) exerted by the fluid on the foil, which in the present nondimensional notation (the force per unit length is scaled

with $1/2\rho U^2 c$) is given by

$$\mathbf{F}(t) = - \int_S p \mathbf{n} dS + \frac{2}{\text{Re}} \int_S \boldsymbol{\omega} \wedge \mathbf{n} dS = F_x \mathbf{e}_x + F_y \mathbf{e}_y, \quad (19)$$

where S is the foil's surface (contour in 2D) oriented with normal vector \mathbf{n} toward the fluid. The x and y components of this force have to be projected onto the parallel and perpendicular axes of the free stream current to obtain the drag and the lift coefficients, respectively, i.e.,

$$C_D(t) = F_x(t) \cos[\alpha(t)] - F_y(t) \sin[\alpha(t)], \quad (20)$$

$$C_L(t) = F_x(t) \sin[\alpha(t)] + F_y(t) \cos[\alpha(t)], \quad (21)$$

and integrating over the oscillating cycle, one obtains the time-averaged values, which for the lift coefficient, if the airfoil does not have an averaged angle over than zero, then it is null and for the thrust coefficient it is given by

$$\bar{C}_T = \frac{1}{T} \int_t^{t+T} C_T(t) dt. \quad (22)$$

Finally, to obtain the pressure on the airfoil surface, a simplified procedure is used based on the pressure gradient along the no-slip surface to the normal derivative of vorticity modified for the noninertial reference frame, i.e.,

$$\frac{1}{2} \nabla p \cdot \mathbf{n}_t = - \frac{1}{\text{Re}} (\nabla \wedge \boldsymbol{\omega}) \cdot \mathbf{n}_t - \left[\mathbf{a}_z + \frac{d\boldsymbol{\Omega}}{dt} \wedge \mathbf{x} + \boldsymbol{\Omega} \wedge (\boldsymbol{\Omega} \wedge \mathbf{x}) \right] \cdot \mathbf{n}_t, \quad (23)$$

where \mathbf{n}_t is the unit tangent vector to the surface of the airfoil. The pressure force at every point on the airfoil is found by assuming an arbitrary value of pressure at one point (the trailing edge) and marching through successive grid points using Eq. (23).

III. NUMERICAL IMPLEMENTATION

The governing equations are discretized using a conformal map. A rectangular, r, θ domain is first mapped to a circular domain using a log-polar transformation [20], and the circular cylinder is mapped into an airfoil by the Kármán-Trefftz transformation,

$$mb \frac{(\zeta + b)^m + (\zeta - b)^m}{(\zeta + b)^m - (\zeta - b)^m} = x + iy, \quad \text{with} \quad \zeta = \zeta_0 + e^{r+i\theta}, \quad (24)$$

where ζ_0 is the location of the cylinder center, $r \in [\log(r_0), \log(r_f)]$, and $\theta \in [0, 2\pi)$, where r_0 is the radius of the cylinder and r_f is the radius end of the meshgrid. With respect to the Kármán-Trefftz transformation, m is related to angle of trailing edge, obtaining the Joukowski profiles when $m = 2$, and b measures the thickness of the airfoil which, for $m = 2$, becomes in a flat plate when $b = 1$ and in a cylinder when $b = 0$. The different values used of the previous parameters are presented in the caption of Fig. 2. The airfoil is constructed fitting a NACA-0012 profile, but to avoid numerical singularities at the trailing edge, it has been rounded as one can see in Fig. 2, where also it has been compared to the actual NACA profile. A portion of the typical mesh is shown in Fig. 3.

The vorticity transport equation in the computational space is given by

$$h_r h_\theta \frac{\partial \boldsymbol{\omega}'}{\partial t} = -(\nabla_{r,\theta} \wedge \psi') \cdot \nabla_{r,\theta} \boldsymbol{\omega}' + \frac{1}{\text{Re}} \nabla_{r,\theta}^2 \boldsymbol{\omega}', \quad (25)$$

where h_r and h_θ are the grid transformation metrics which links the physical (x, y) space with the computational (r, θ) space. The subscripts r, θ refer to derivatives in the r, θ domain.

The Poisson equation for ψ' becomes

$$\nabla_{r,\theta}^2 \psi' = -h_r h_\theta \boldsymbol{\omega}'. \quad (26)$$

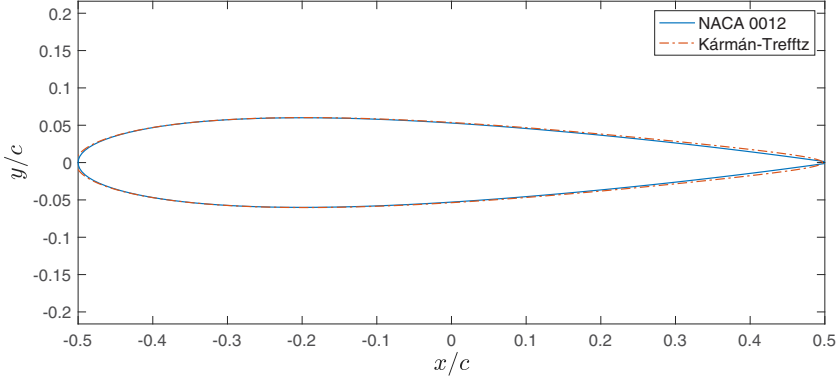


FIG. 2. Comparison of the NACA-0012 profile with Kármán-Trefftz profile. The values of the parameters are $\zeta_0 = -0.01765$, $r_0 = 0.29$, $m = 2.0257$, and $b = 0.2566$ with a goodness-of-fit of $R^2 = 0.9971$.

One must take into account that $h_r = h_\theta$ as a result of the log-polar transformation in the first mapping to a circular domain, turning the governing equations into Cartesian equations multiplied by the factor $h_r h_\theta$. After spatial discretization, the semidiscrete scheme Eq. (25) is equivalent to the first ODE system, i.e.,

$$\frac{\partial \omega'}{\partial t} = R(\omega'), \quad \text{with} \quad R(\omega') = \frac{1}{h_r h_\theta} \left[\frac{1}{\text{Re}} \left(\frac{\partial^2 \omega'}{\partial r^2} + \frac{\partial^2 \omega'}{\partial \theta^2} \right) - \frac{\partial \psi}{\partial r} \frac{\partial \omega'}{\partial \theta} + \frac{\partial \psi}{\partial \theta} \frac{\partial \omega'}{\partial r} \right], \quad (27)$$

and the Poisson equation for the stream function Eq. (26) yields

$$\frac{\partial^2 \psi'}{\partial r^2} + \frac{\partial^2 \psi'}{\partial \theta^2} = -h_r h_\theta \omega', \quad (28)$$

where the spatial discretization is carried out on a uniform grid of width Δ in both r and θ directions.

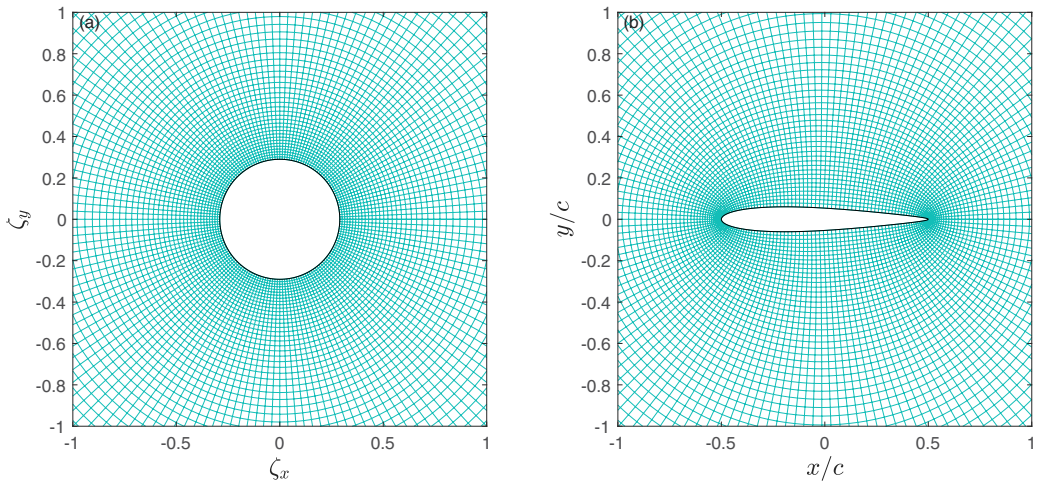


FIG. 3. A portion of the generated grid in the circular domain (a) and in the physical space (b) for the parameters $\zeta_0 = -0.01765$, $r_0 = 0.29$, $m = 2.0257$, and $b = 0.2566$ with a uniform grid spacing of $\Delta = \pi/80$ in the (r, θ) plane.

A. Discretization and initial condition

For time marching, a second-order Runge-Kutta scheme is used for the vorticity transport equation. For spatial terms, sixth-order compact centered scheme differencing is used [21]. For easy reference, the first and second derivatives, $\partial f/\partial\theta$ and $\partial^2 f/\partial\theta^2$, are given, respectively, by

$$\frac{1}{3}f'_{i,j-1} + f'_{i,j} + \frac{1}{3}f'_{i,j+1} = \frac{14}{9} \frac{f_{i,j+1} - f_{i,j-1}}{2\Delta} + \frac{1}{9} \frac{f_{i,j+2} - f_{i,j-2}}{4\Delta}, \quad (29)$$

$$\frac{2}{11}f''_{i,j-1} + f''_{i,j} + \frac{2}{11}f''_{i,j+1} = \frac{12}{11} \frac{f_{i,j-1} - 2f_{i,j} + f_{i,j+1}}{\Delta^2} + \frac{2}{11} \frac{f_{i,j-2} - 2f_{i,j} + f_{i,j+2}}{4\Delta^2}. \quad (30)$$

In the case of the first and second derivatives in the radial direction, $\partial f/\partial r$ and $\partial^2 f/\partial r^2$, the nodes $i = 1$, $i = 2$, $i = N_r$, and $i = N_r - 1$ have to be approximated with forward or backward compact finite differences (where N_r is the total number of nodes in the radial direction of the meshgrid), i.e.,

(i) $i = 1$

$$f' + 5f'_2 = \frac{1}{\Delta} \left[-\frac{197}{60}f_1 - \frac{5}{12}f_2 + 5f_3 - \frac{5}{3}f_4 + \frac{5}{12}f_5 - \frac{1}{20}f_6 \right], \quad (31)$$

$$f'' + \frac{126}{11}f''_2 = \frac{1}{\Delta^2} \left[\frac{13097}{990}f_1 - \frac{2943}{110}f_2 + \frac{573}{44}f_3 + \frac{167}{99}f_4 - \frac{18}{11}f_5 + \frac{57}{110}f_6 - \frac{131}{1980}f_7 \right], \quad (32)$$

(ii) $i = 2$

$$\frac{2}{11}f'_1 + f'_2 + \frac{2}{11}f'_3 = \frac{1}{\Delta} \left[-\frac{20}{33}f_1 - \frac{35}{132}f_2 + \frac{34}{33}f_3 - \frac{7}{33}f_4 + \frac{2}{33}f_5 - \frac{1}{132}f_6 \right], \quad (33)$$

$$\frac{11}{128}f''_1 + f''_2 + \frac{11}{128}f''_3 = \frac{1}{\Delta^2} \left[\frac{585}{512}f_1 - \frac{141}{64}f_2 + \frac{459}{512}f_3 + \frac{9}{32}f_4 - \frac{81}{512}f_5 + \frac{3}{64}f_6 - \frac{3}{512}f_7 \right]. \quad (34)$$

For $i = N_r$ and $i = N_r - 1$, the compact finite-difference coefficients are the same for the second derivative and with the opposite sign for the first derivative on the right-hand side but taking into account that the evaluation has to be done in the backward direction ($i = N_r, \dots, N_r - 6$, for the right-hand side). Note that the factor 2077/157 in the first term of the second derivative for $i = 1$ on the right-hand side reported in Ref. [21] has been corrected in Eq. (32).

For the Poisson equation for the stream function, the equations are discretized using a sixth-order compact centered scheme [22] and solved using a strongly implicit procedure solver with a Cholesky factorization. For the boundary condition on the airfoil surface in the case of the vorticity is used the fourth-order Briley formula [23], i.e.,

$$\omega'_a = \frac{1}{18\Delta n^2} [85\psi_a - 108\psi_{a+1} + 27\psi_{a+2} - 4\psi_{a+3}] + 2\Omega. \quad (35)$$

On the other hand, in order to avoid nonphysical starting flows when simulating a flapping motion, the permanent von Kármán vortex street wake behind the airfoil is previously obtained when it is horizontally at rest.

B. Mesh convergence and validation of the code

A grid sensitivity analysis was performed using three or more meshes for every considered Reynolds number and setting up $a = -0.25$, $a_0 = 2^\circ$, and with $St = 0.4$, which is the highest value of the Strouhal number considered in the present study and therefore the most adverse case in terms of trailing edge velocity. After a large number of simulations, it is selected a specific grid size for every considered Reynolds number in the present study in order to optimize the computational cost assuming a relative error below 2%, where $\Delta = \pi/300$ for the lower case ($Re = 500$) and $\Delta = \pi/800$ for the highest Reynolds number ($Re = 8000$) (see Fig. 4), with a the time step

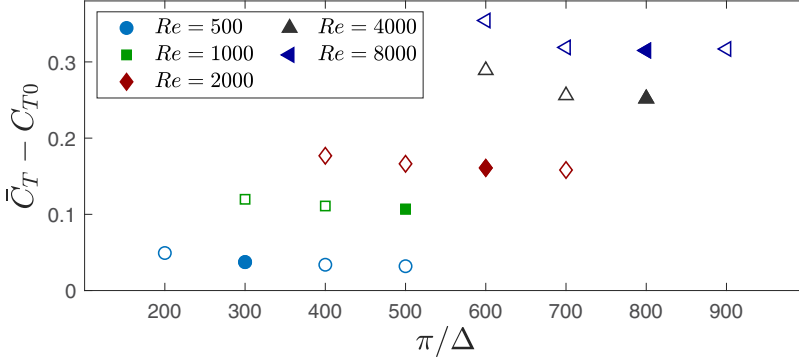


FIG. 4. Grid convergence study of the time-averaged thrust coefficient relative to the constant value C_{T0} for the different Reynolds numbers considered in the present study with the selected grid spacing, Δ (filled markers) when $a = -0.25$, $a_0 = 2^\circ$, and with $St = 0.4$. Numerical simulations with 50 periods and time-averaged values computed over the last five cycles.

$\Delta t \sim 10^{-5}$. Apart from that, the Appendix reports the validation of the code with a impulsively started cylinder for several Reynolds numbers, comparing the closed wake length, the location of the main eddy core, and the velocity at the mean line of the cylinder wake with the theory and the experimental results from Ref. [24]. In addition, the temporal evolution of the lift coefficient for pure heaving motion of the considered airfoil for $Re = 10\,000$, $h_0 = 0.025$, and $k = 7.86$ has been compared with the experimental results of Ref. [3], the numerical results of Ref. [6], and the theoretical ones in Ref. [7].

IV. RESULTS

A. Pure pitching motion

As first numerical results, the model described above is used to simulate a pitching airfoil ($h_0 = 0$), pivoting to a quarter chord length, $a = -0.25$, with a pitching amplitude of $a_0 = 2^\circ$. The Strouhal number ranges from $0.05 \leq St \leq 0.4$, i.e., varying the reduced frequency from $3 \lesssim k \lesssim 24$ [see the Eq. (7)] for various Reynolds numbers. In Fig. 5(a) one can see the time-averaged thrust coefficient relative to the constant thrust value, C_{T0} , which is the time-averaged thrust coefficient

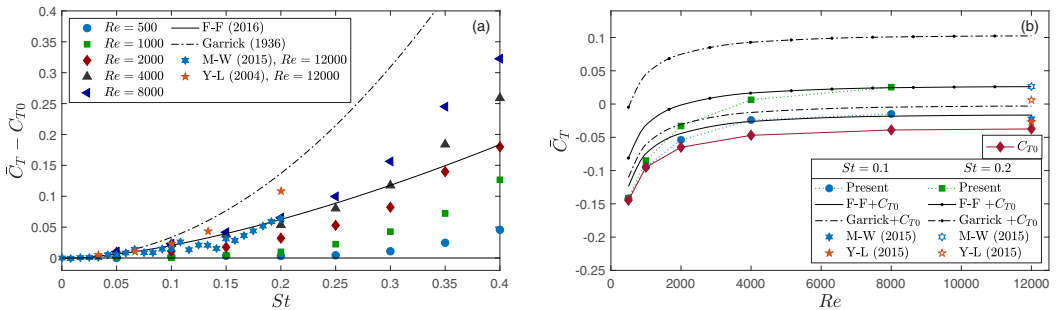


FIG. 5. (a) Comparison of the time-averaged thrust relative to the constant value C_{T0} with the experimental results from Ref. [5] (M-W in the legend) and the numerical from Ref. [25] and the theoretical ones in Ref. [8] and Ref. [9] (F-F in the legend) for various Reynolds numbers. (b) Time-averaged thrust as a function of the Reynolds number for two values of the Strouhal number together with the value of C_{T0} . Pure pitching motion with $a_0 = 2^\circ$ and $a = -0.25$.

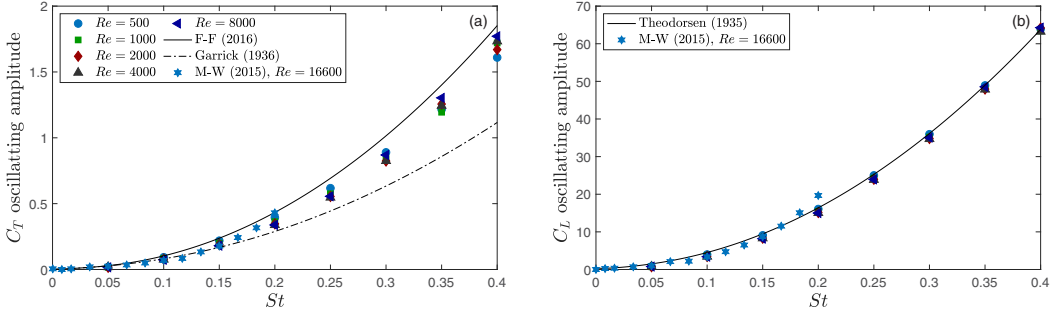


FIG. 6. Comparison of the thrust (a) and lift (b) oscillating amplitude with the experimental results from Ref. [5] and the theoretical results in Ref. [8] and Ref. [9] for the thrust and in Ref. [7] for the lift with various Reynolds number. Pure pitching motion with $a_0 = 2^\circ$ and $a = -0.25$.

value that tends to result when $k \rightarrow 0$ [10]. Together with the present numerical results, the experimental results from Ref. [5] for $Re = 12\,000$ are plotted. Also, the previously mentioned theoretical models [8,9] have been plotted [from now on the Garrick and F-F (Fernandez-Feria) models, respectively] in comparison with the numerical and experimental results. The F-F theory predicts the numerical and experimental results better than the classical Garrick theory, where the F-F theory is limited for values of the Strouhal number $St \lesssim 0.25$ and for values of the Reynolds number $Re \gtrsim 4000$, since the relative time-averaged thrust value does not change for high Reynolds number, as can be seen in the Fig. 5(b). This effect has been found also for high pitching amplitudes [18].

On the other hand, the theoretical results of the F-F model compare better than the Garrick ones not only in the case of time-averaged values but also for the thrust oscillating amplitudes as one can see in the Fig. 6(a) showing this effect more clearly for high values of the Strouhal number. In the case of the lift coefficient oscillating amplitude, the numerical results collapse with the theory from Ref. [7] [see Fig. 6(b)]. Recent findings show that $C_T - C_{T0}$ should scale with St^2 [18,26], but to be consistent with the linear theories, the unsteady thrust amplitude has been normalized by the square of the pitching angle [see Fig. 7(a)]. Nevertheless, in the Fig. 7(b), the corresponding phase lag in the thrust coefficient normalized with St^2 has been plotted in regard to $\sin(4kt)$ to compare with the experimental results from Ref. [5]. As can be seen, the F-F model predicts slightly better a C_T oscillating amplitude independent of a_0 , but both theories scale the phase lag with St^2 .

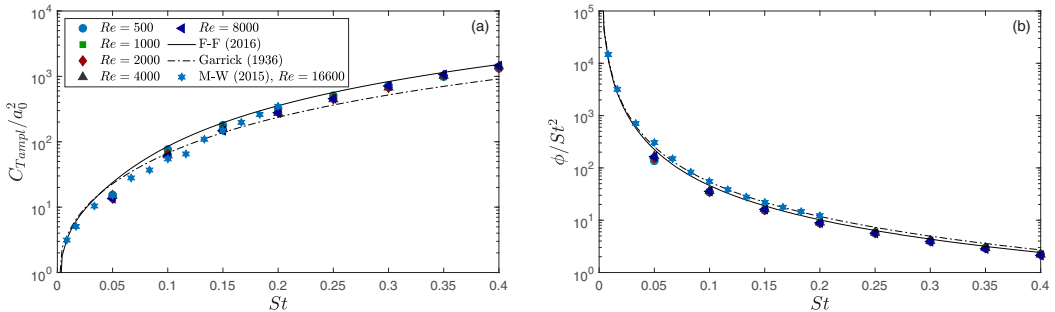


FIG. 7. Comparison of the thrust oscillating amplitude normalized with a_0^2 (a) and the phase lag normalized with St^2 (b) with the experimental results from Ref. [5] and the theoretical results in Ref. [8] and Ref. [9] for various Reynolds number. Pure pitching motion with $a_0 = 2^\circ$ and $a = -0.25$.

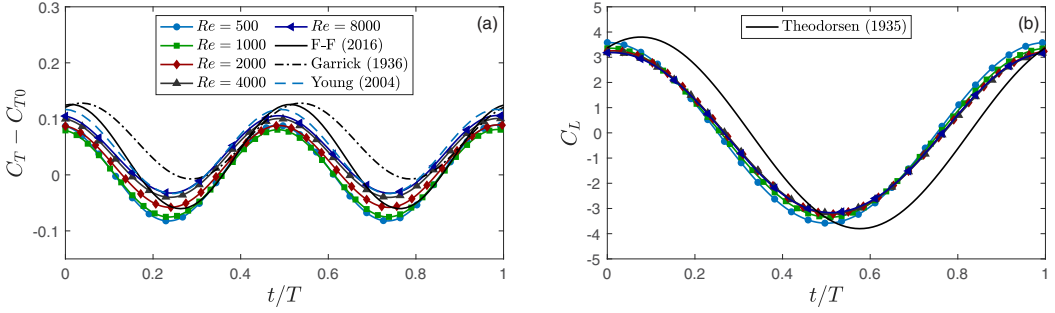


FIG. 8. (a) Comparison of the time evolution of the thrust coefficient relative to C_{T0} with the numerical results from Ref. [25] and the theoretical results in Ref. [8] and Ref. [9], F-F in the legend. (b) Comparison of the temporal evolution of the lift coefficient with the theoretical results from Ref. [7]. Pure pitching motion with $a_0 = 2^\circ$, $a = -0.25$, $k = 8$ ($St \simeq 0.133$) and the considered values of the Reynolds number.

In Fig. 8(a) for the selected case of $k = 8$ ($St \simeq 0.133$), the oscillating amplitude of the thrust coefficient has been plotted, where F-F model compares better than the Garrick model, and the Garrick theory presents a bigger lag in the temporal evolution of the thrust coefficient. Together with the present results the numerical results from Ref. [25] for $Re = 12\,000$ are plotted, showing that for high Reynolds numbers, the thrust coefficient relative to the constant thrust value, C_{T0} , practically does not change. Also, the temporal evolution of the lift coefficient is plotted in Fig. 8(b) for the considered values of the Reynolds number comparing with the theoretical results from Ref. [7], As shown in Fig. 6(b), the numerical results are practically independent of the Reynolds number and the oscillating amplitude of C_L coincides with the theoretical results. However, as one can see in Fig. 8(b) the theory lags behind the numerical results.

Finally, in Fig. 9(a) the time-averaged thrust coefficient has been plotted varying the pivot point location for the selected case of $St = 0.2$, relative to the constant value $C_{T0}^* = \bar{C}_T(St = 0.05)$ [see Fig. 9(b)] as an approximation of C_{T0} . Note that for $a = -0.5$ the pivot point is located in the leading edge, and when $a = 0.5$, it is in the trailing edge. The collapse of the time-averaged thrust coefficient for high Reynolds number is produced also varying the pivot point location, and once again, the F-F model predicts better the numerical results than the Garrick model.

B. Pure heaving motion

As second numerical results, a pure heaving motion ($a_0 = 0$) has been considered, with a plunging amplitude of $h_0 = 0.025$. The Strouhal number ranges from $0.05 \leq St \leq 0.4$, i.e., varying

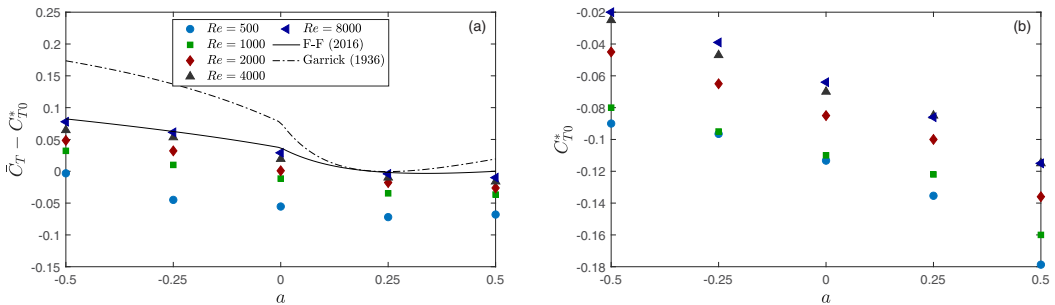


FIG. 9. (a) Comparison of the time-averaged thrust relative to the constant value C_{T0}^* (b) with the theoretical results in Ref. [8] and Ref. [9] for various Reynolds numbers and varying the pivot point location for $St = 0.2$ and $a_0 = 2^\circ$.

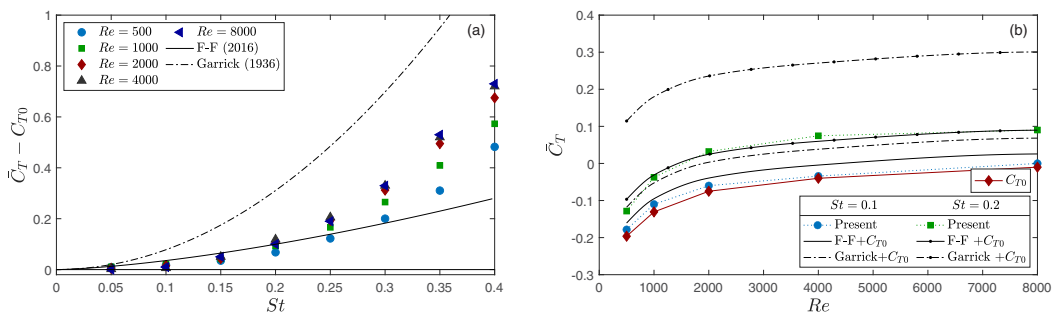


FIG. 10. (a) Comparison of the time-averaged thrust relative to the constant value C_{T0} with the theoretical ones in Ref. [8] and Ref. [9], F-F in the legend, for various Reynolds number. (b) Time-averaged thrust as a function of the Reynolds number for two values of the Strouhal number together with the value of C_{T0} . Pure heaving motion with $h_0 = 0.025$.

the reduced frequency from $\pi \leq k \leq 8\pi$ [see the Eq. (7)] for the same Reynolds numbers in the case of pure pitching motion. In this case, the F-F theory is limited for values of the Strouhal number $St \lesssim 0.2$ as one can see in Fig. 10(a). For bigger heaving amplitudes, it has been found that the limitation of the theory is reached for $St \lesssim 0.3$ as has been reported in Ref. [9] and later in Ref. [6]. Apart from that, for pure heaving motion, the theory can be used for smaller Reynolds numbers than for pure pitching motion as one can see in the Fig. 10(b) more clearly. However, the thrust coefficient oscillating amplitude is predicted better by the Garrick theory than the F-F theory [see Fig. 11(a)], in spite of the lift coefficient oscillating amplitude, which is still well reproduced in Ref. [7] [see Fig. 11(b)]. Note that, although the Garrick theory compares better than the F-F theory for the oscillating amplitude of the thrust coefficient, the time-averaged thrust coefficient continues matching better with the F-F theory, as has been mentioned before. On the other hand, one has to take into account that for values of the Strouhal number $St \gtrsim 0.3$, the solution is aperiodic and the time-averaged thrust coefficient depends on the number of flapping cycles which one uses to obtain the mean, as for bigger heaving amplitudes shown in Ref. [6].

C. Combined motions

Both linear potential theories make the assumption of considering small oscillating amplitudes as has been mentioned before. Nonetheless, the F-F theory still continues to predict better the numerical or experimental results even when the oscillating amplitudes are not small. To show that,

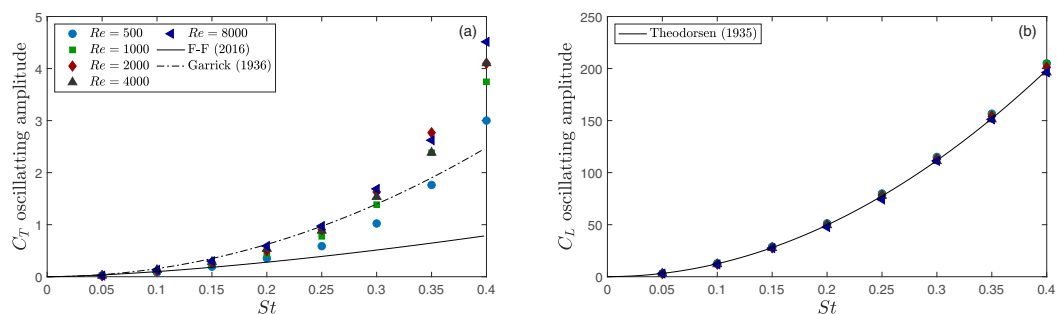


FIG. 11. Comparison of the thrust (a) and lift (b) oscillating amplitude with the theoretical results in Ref. [8] and Ref. [9] for the thrust and in Ref. [7] for the lift with various Reynolds number. Pure heaving motion with $h_0 = 0.025$.

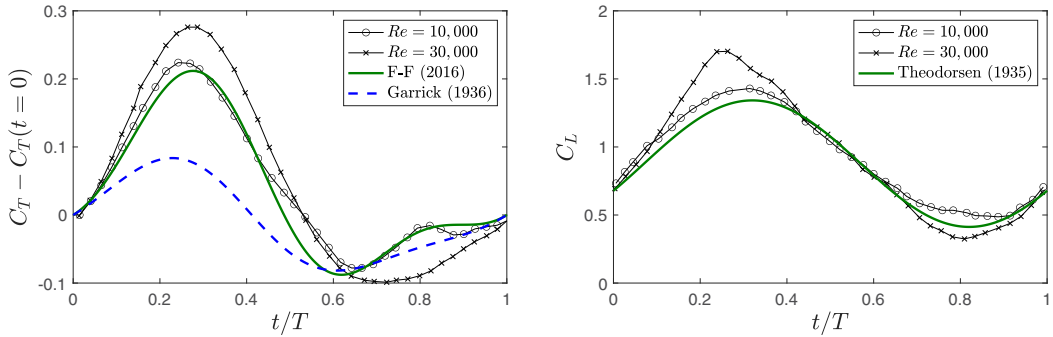


FIG. 12. Comparison of the theoretical results with the experimental results from Ref. [4] of the time evolution of the thrust and lift coefficient for $k = 0.25$, $h_0 = 0.5$, $a_0 = 8.42^\circ$, $\phi = \pi/2$, and $\alpha_m = 8^\circ$ ($St \simeq 0.08$).

the theoretical results have been compared for a combined motion with an averaged angle greater than zero, α_m , with the experimental results from Ref. [4] for a flat plate. Although this case has not been simulated because the mesh convergence would have to be done again for this particular case, it is interesting to show the better agreement of the F-F theory for not-small oscillating amplitudes compared to the Garrick theory when a $\alpha_m \neq 0$ is considered. The kinematics parameters of this motion are given in the caption to Fig. 12. Note that, to compare correctly these experimental results with the theory, one has to add the steady lift contribution, $C_{L0} = 2\pi\alpha_m$, and consequently to remove the contribution of the mean angle in the plate circulation. As one can see in Fig. 12, the theoretical results of the F-F model are still much better than those of the Garrick model even when the $\alpha_m \neq 0$ and the motion amplitudes are not small. Nonetheless, for very high Reynolds numbers, the theoretical results begin to not compare well with the experimental results because of the turbulence effects in these large motion amplitudes.

V. CONCLUSION

A two-dimensional numerical model has been presented to compute the flapping motion of an airfoil, using the Kármán-Trefftz transformation fitting a NACA profile. The governing equations have been solved with a compact finite-differences scheme of sixth order in terms of vorticity and stream function, which has been validated with different experimental, numerical, and theoretical results.

The numerical simulation of a flapping airfoil has been used to find the validity limit of two theoretical models given in Ref. [8] and Ref. [9], respectively, in terms of Reynolds and Strouhal numbers for pure pitching motion and for pure heaving motion. In general terms, the F-F theory

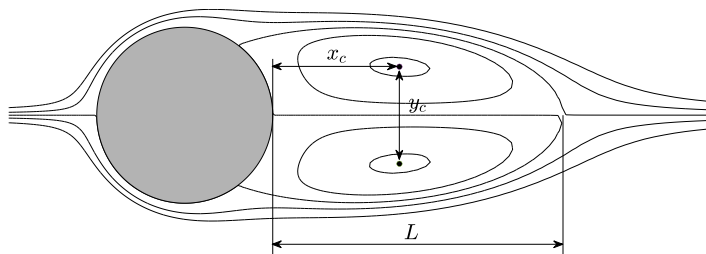


FIG. 13. Definition of the characteristic dimensions of the wake structure of the flow around the circular cylinder.

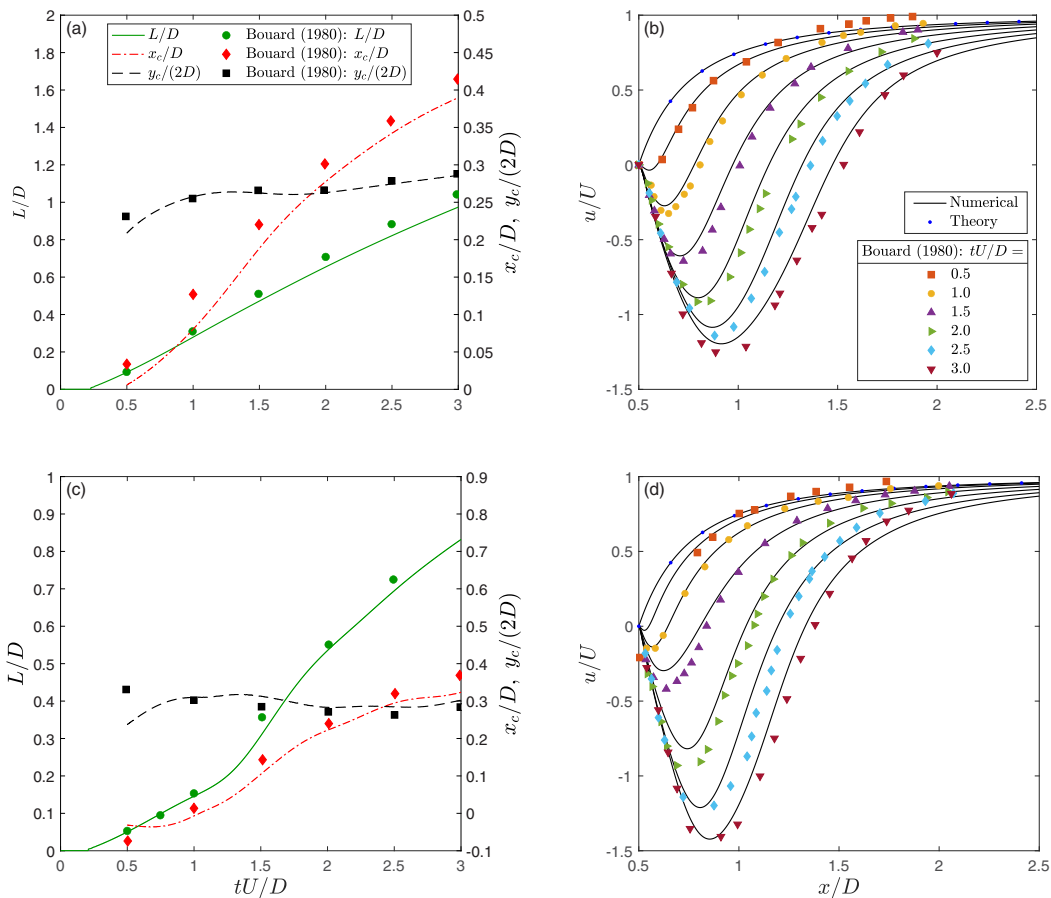


FIG. 14. Comparison of the numerical results with the experimental data from Ref. [24], for $Re = 550$ (a) and for $Re = 3000$ (c), of the closed wake length, L/D , and location of the main eddy core, x_c/D , $y_c/(2D)$ (measured from the most downstream point of the cylinder). Numerical results (continuous line) for the velocity at the mean line of the wake compared with the theory (dots), and the experimental data from Ref. [24], for several moments of time (see the legend of the figure) for $Re = 550$ (b) and for $Re = 3000$ (d).

presents better results for time-averaged coefficients than for time-dependent coefficients for the case of pure pitching motion. Also, it has been found that the F-F theory could be used when the Reynolds number is greater than 4000 and $St \lesssim 0.25$. However, only the Garrick theory matches with the numerical results for small values of the Strouhal number, when it is computing the time-averaged thrust coefficient. In the case of pure heaving motion, the Reynolds number limitation is smaller than the case of pure pitching motion, i.e., the F-F theory could be used from $Re \gtrsim 1000$ and $St \lesssim 0.2$, although for large heaving amplitudes, the Strouhal number limitation could be greater ($St \lesssim 0.3$) [6]. On the other hand, the Garrick theory compares better than the F-F theory for the oscillating amplitude of the thrust coefficient, but the time-averaged thrust coefficient continues to match better with the F-F theory. In order to correctly compare both linearized theoretical models with the experimental and numerical results it is necessary to add the quasisteady constant thrust value, C_{T0} [10], when it is computing the time-averaged thrust coefficient, which must be obtained numerically or experimentally. Finally, the F-F theory still works better than the Garrick theory even when the flapping amplitudes are large and with an averaged angle over than zero.

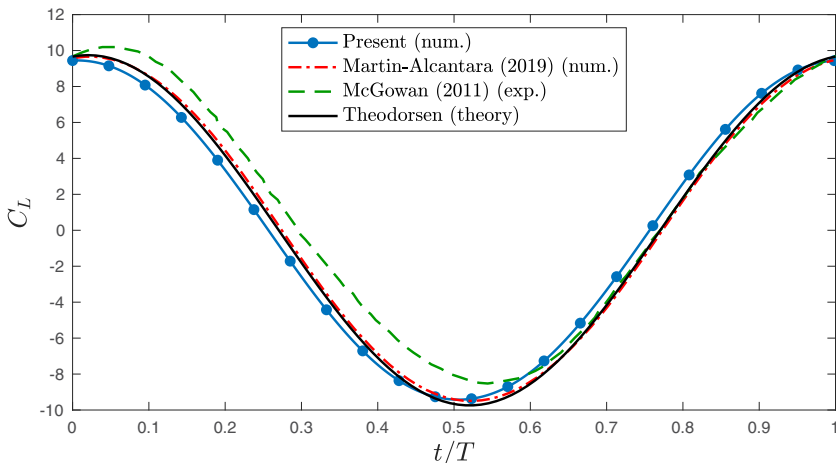


FIG. 15. Lift coefficient $C_L(t)$ during a cycle compute for $Re = 10\,000$, $h_0 = 0.025$, and $k = 7.86$ compared with the experimental results of Ref. [3], the numerical results of Ref. [6], and the theoretical ones in Ref. [7].

ACKNOWLEDGMENTS

This research was supported by the Ministerio de Economía y Competitividad of Spain Grant No. DPI2016-76151-C2-1-R. The computations were performed in the Picasso Supercomputer at the University of Málaga, a node of the Spanish Supercomputing Network.

APPENDIX: VALIDATION OF THE CODE

To validate the code and test that it is working correctly, some numerical simulations have been done comparing with experimental available results in the bibliography. Firstly, the numerical simulations have been compared with the flow around a circular cylinder where the characteristic dimensions of the wake structure are defined in Fig. 13. In Figs. 14(a) and 14(c), one can see the comparison of the closed wake length and the location of the main eddy core for $Re = 550$ and $Re = 3000$. Given the three-dimensional nature of the experimental problem and the difference in starting conditions, the agreement is very good.

In addition, the velocity at the mean line of the cylinder wake has been compared with the theory and the experimental results from Ref. [24] for the same flow conditions as above. Figures 14(b) and 14(d) show a comparison between computed and experimental flows with very good agreement.

Finally, Fig. 15 shows a comparison of the lift coefficient $C_L(t)$ during a cycle, computed for $Re = 10\,000$, $h_0 = 0.025$, and $k = 7.86$ for a pure heaving motion with the experiments from Ref. [3], the numerical simulations from Ref. [6], and the theory in Ref. [7] in order to test the conformal mapping fitting the NACA profile. Again the agreement is very good.

-
- [1] M. F. Platzer, K. D. Jones, J. Young, and J. C. Lai, Flapping-wing aerodynamics: Progress and challenges, *AIAA J.* **46**, 2136 (2008).
 - [2] W. Shyy, H. Aono, C. K. Kang, and H. Liu, *An Introduction to Flapping Wing Aerodynamics* (Cambridge University Press, Cambridge, 2013).
 - [3] G. Z. McGowan, K. Granlund, M. V. Ol, A. Gopalarathnam, and J. R. Edwards, Investigations of lift-based pitch-plunge equivalence for airfoils at low Reynolds numbers, *AIAA J.* **49**, 1511 (2011).

-
- [4] Y. S. Baik and L. P. Bernal, Experimental study of pitching and plunging airfoils at low Reynolds numbers, *Exp. Fluids* **53**, 1979 (2012).
- [5] A. W. Mackowski and C. H. K. Williamson, Direct measurement of thrust and efficiency of an airfoil undergoing pure pitching, *J. Fluid Mech.* **765**, 524 (2015).
- [6] A. Martín-Alcántara and R. Fernández-Feria, Assessment of two vortex formulations for computing forces of a flapping foil at high Reynolds numbers, *Phys. Rev. Fluids* **4**, 024702 (2019).
- [7] T. Theodorsen, General theory of aerodynamic instability and the mechanism of flutter, Technical Report TR 496, NACA (1935); L. Vinet and A. Zhedanov, A ‘missing’ family of classical orthogonal polynomials, *J. Phys. A: Math. Theor.* **44**, 085201 (2011).
- [8] I. E. Garrick, Propulsion of a flapping and oscillating airfoil, Technical Report TR 567, NACA (1936).
- [9] R. Fernández-Feria, Linearized propulsion theory of flapping airfoils revisited, *Phys. Rev. Fluids* **1**, 084502 (2016).
- [10] R. Fernández-Feria, Note on optimum propulsion of heaving and pitching airfoils from linear potential theory, *J. Fluid Mech.* **826**, 781 (2017).
- [11] R. Fernández-Feria and J. Alaminos-Quesada, Unsteady thrust, lift and moment of a two-dimensional flapping thin airfoil in the presence of leading-edge vortices: A first approximation from linear potential theory, *J. Fluid Mech.* **851**, 344 (2018).
- [12] J. Alaminos-Quesada and R. Fernández-Feria, Propulsion of a foil undergoing a flapping undulatory motion from the impulse theory in the linear potential limit, *J. Fluid Mech.* **883**, A19 (2020).
- [13] T. H. von Kármán and W. R. Sears, Airfoil theory for non-uniform motion, *J. Aeronaut. Sci.* **5**, 379 (1938).
- [14] J. C. Wu, Theory for aerodynamic force and moment in viscous flows, *AIAA J.* **19**, 432 (1981).
- [15] A. A. Tchieu and A. Leonard, A discrete-vortex model for the arbitrary motion of a thin airfoil with fluidic control, *J. Fluids Struct.* **27**, 680 (2011).
- [16] R. Fernández-Feria and E. Sanmiguel-Rojas, Comparison of aerodynamic models for two-dimensional pitching foils with experimental data, *Phys. Fluids* **31**, 057104 (2019).
- [17] R. Fernández-Feria and E. Sanmiguel-Rojas, Effect of the pivot point location on the propulsive performance of a pitching foil, *J. Fluids Struct.* **97**, 103089 (2020).
- [18] U. Senturk and A. J. Smits, Reynolds number scaling of the propulsive performance of a pitching airfoil, *AIAA J.* **57**, 2663 (2019).
- [19] G. C. LEWIN and H. HAJ-HARIRI, Modelling thrust generation of a two-dimensional heaving airfoil in a viscous flow, *J. Fluid Mech.* **492**, 339 (2003).
- [20] C. L. Lin, D. W. Pepper, and S. C. Lee, Numerical methods for separated flow solutions around a circular cylinder, *AIAA J.* **14**, 900 (1976).
- [21] M. Mehra and K. S. Patel, Algorithm 986: A suite of compact finite difference schemes, *ACM Trans. Math. Softw.* **44**, 1 (2017).
- [22] G. Sutmann, Compact finite difference schemes of sixth order for the Helmholtz equation, *J. Comput. Appl. Math.* **203**, 15 (2007).
- [23] W. R. Briley, A numerical study of laminar separation bubbles using the Navier-Stokes equations, *J. Fluid Mech.* **47**, 713 (1971).
- [24] R. Bouard and M. Coutanceau, The early stage of development of the wake behind an impulsively started cylinder for $40 < Re < 10^4$, *J. Fluid Mech.* **101**, 583 (1980).
- [25] J. Young and J. C. Lai, Oscillation frequency and amplitude effects on plunging airfoil propulsion and flow periodicity, *AIAA J.* **42**, 10 (2004).
- [26] D. Floryan, T. Van Buren, C. W. Rowley, and A. J. Smits, Scaling the propulsive performance of heaving and pitching foils, *J. Fluid Mech.* **822**, 386 (2017).